

1 **CORRELATION BETWEEN TECTONIC STRESS REGIMES AND METHANE SEEPAGE ON THE**
2 **WEST-SVALBARD MARGIN**

3
4 A. Plaza-Faverola¹ and M. Keiding²

5 ¹ CAGE-Centre for Arctic Gas Hydrate, Environment, and Climate; Department of Geosciences, UiT The Arctic
6 University of Norway, N-9037 Tromsø, Norway

7 ² Geological Survey of Norway (NGU), P.O. Box 6315 Torgarden, 7491 Trondheim, Norway

8 *Correspondence to:* Andreia Plaza-Faverola (Andreia.a.faverola@uit.no)

9 **Abstract.** Methane seepage occurs across the west-Svalbard margin at water depths ranging from the upper shelf
10 at < 300 m to gas hydrate systems in the deep sea at > 1000 m. The Vestnesa sedimentary ridge, located on oceanic
11 crust at 1000-1700 m water depth, hosts a perennial gas hydrate and associated free gas system. Present day seepage
12 activity is restricted to the eastern segment of the sedimentary ridge, despite morphological and paleontological
13 evidence for past seepage activity along the entire ridge extent. An eastward transition from the zone with clear
14 morphological evidence of past seepage to the zone of active present-day seepage coincides with a change in the
15 faulting pattern of near-surface strata. We modelled the tectonic stress regime exclusively due to oblique spreading
16 along the Molloy and Knipovich spreading ridges to investigate whether spatial and temporal variations in the
17 spreading-related stress field may explain patterns of seepage distribution. The model reveals a zone of tensile
18 stress that extends northward from the Knipovich Ridge and encompasses the zone of extensional faulting and
19 associated active seepage on the eastern Vestnesa Ridge segment. The seemingly inactive part of the ridge is
20 presently located in a strike-slip regime. Our modelling results suggest that present-day seepage can be explained
21 by opening of faults and fractures favourably oriented with respect to spreading-related principal stresses, where
22 pore fluid pressure overcomes the horizontal stress. Multiple seepage events along the entire extent of the gas-
23 charged Vestnesa Ridge, may have been incited by favourably oriented mid-ocean ridge derived-stresses in the past
24 or by additional sources of stress related for example to glacial isostasy. Our study provides a first order assessment
25 of how stresses from mid-ocean ridge spreading may be influencing the kinematics of near-surface faults and
26 associated seepage activity offshore the west-Svalbard passive margin.

27

28

29 1. INTRODUCTION

30 Seafloor seepage is a wide-spread phenomenon which consists in the release of natural gases into the oceans.
31 Hundreds of gigatonnes of carbon are stored as gas hydrates and shallow gas reservoirs in continental margins (e.g.,
32 Hunter et al., 2013). The release of these carbons over geological time is an important component of the global
33 carbon cycle. Understanding and quantifying seepage has important implications for ocean acidification, deep-sea
34 ecology and global climate. Periods of massive methane release from gas hydrate systems (e.g., Dickens, 2011) or
35 from large volcanic basins like that in the mid-Norwegian Margin (e.g., Svensen et al., 2004) have been linked to
36 global warming events such as the Palaeocene-Eocene thermal maximum. We know that methane seepage has been
37 occurring for millions of years, but we have a poor understanding of what forces it.

38

39 Present day seepage is identified as acoustic flares in the water column commonly originating at seafloor
40 depressions, while authigenic carbonate mounds are used as indicators of longer-term seepage activity (e.g., Judd
41 and Hovland, 2009). Seepage at the theoretical upstream termination of the gas hydrate stability zone (GHSZ) (i.e.,
42 coinciding with the shelf edge) on different continental margins, has been explained by temperature driven gas-
43 hydrate dissociation (e.g., Skarke et al., 2014; Westbrook et al., 2009). On formerly glaciated margins, active
44 seepage is believed to be associated with pressure changes resulting from the retreat of the ice-sheet (e.g.,
45 Andreassen et al., 2017; Portnov et al., 2016). The effect of post-glaciation uplift on gas hydrate stability has been
46 recently suggested as an alternative explanation for seepage localized at the shelf break offshore west-Svalbard
47 (Wallmann et al., 2018)

48

49 Across the formerly glaciated west-Svalbard margin, active seepage extends beyond the shelf break and the region
50 formerly covered by ice. As a matter of fact, active seepage sites have been identified from inside Isfjorden (Roy
51 et al., 2014) to water depths of ~1200 m (Smith et al., 2014) where the Vestnesa Ridge hosts a perennially stable
52 gas hydrate system beyond the ice-sheet grounding line. The Vestnesa Ridge is a NW-SE oriented contourite
53 deposit located between the northward termination of the Knipovich ridge and the eastern flank of the Molloy
54 spreading ridge in the Fram Strait (Fig. 1). Seafloor pockmarks along the Vestnesa Ridge, first documented by
55 Vogt (1994), exist along the entire ridge. However, acoustic flares have been observed to originate exclusively at
56 large pockmarks located on the eastern part of the sedimentary ridge (Fig. 2, 3). The presence of inactive pockmarks
57 adjacent to a zone of active seepage along the Vestnesa Ridge, raises the question what stopped previously active
58 seepage sites?

59

60 Plaza-Faverola et al., (2015) documented seismic differences in the orientation and type of faulting along the ridge
61 and showed a link between the distribution of gas chimneys and faults. They postulated that spatial and temporal
62 tectonic stress variations have a long-term effect on the spatial distribution of fault-related gas migration and
63 seepage evolution. The information about the present day stress regime in the Fram Strait is limited to large scale
64 lithospheric density models (Schiffer et al., 2018) and a limited number of poorly constrained stress vectors from
65 earthquake focal mechanisms (Heidbach et al., 2010). Here, we experiment with an approach that allows us to
66 approximate the orientation and type of stress regimes exclusively due to oblique spreading at Molloy and
67 Knipovich Ridges. We study, qualitatively, how stresses from mid-ocean ridge spreading alone may be influencing
68 the kinematics of near-surface faults and associated methane seepage activity along the Vestnesa Ridge.

69

70 The effect of regional stresses on fluid dynamics in the near-surface has implications for seepage systems globally.
71 The relationship between fault kinematics and fluid migration has been documented specially at accretionary
72 margins where earthquake-induced seafloor seepage has been monitored (e.g., Geersen et al., 2016) and splay-
73 faults are found to sustain shallow gas accumulations and seepage (Plaza-Faverola et al., 2016). With the present
74 study we show, using an Arctic case, that seepage on passive continental margins may be affected as well by the
75 stress regime resulting from mid-ocean ridge spreading.

76

77 **2. STRUCTURAL AND STRATGRAPHIC SETTING OF THE VESTNESA RIDGE**

78 In Fram Strait, sedimentary basins are within tens of kilometres from ultra-slow spreading Arctic mid-ocean ridges
79 (Fig. 1). The opening of the Fram Strait was initiated 33 Ma ago and evolved as a result of slow spreading of the
80 Molloy and Knipovich Ridges (Engen et al., 2008). An important transpressional event deformed the sedimentary
81 sequences of western Svalbard, resulting in folds and thrustbelts, during the Paleocene-Eocene dextral movement
82 of Spitsbergen with respect to Greenland. Transpression stopped in the early Oligocene when the tectonic regime
83 became dominated by extension (Myhre and Eldholm, 1988). The circulation of deep water masses through Fram
84 Strait started during the Miocene, ca. 17-10 Ma ago (Ehlers and Jokat, 2009; Jakobsson et al., 2007), establishing
85 the environmental conditions for the evolution of bottom current-driven sedimentary drifts (Eiken and Hinz, 1993;
86 Johnson et al., 2015). It has been suggested that the opening of the northern Norwegian–Greenland Sea was initiated
87 by the northward propagation of the Knipovich ridge into the ancient Spitsbergen Shear Zone (SSZ) (Crane et al.,
88 1991) .

90 The continental crust beneath the western coast of Svalbard thins towards the Hornsund Fault zone (HFZ) indicating
91 extension following the opening of the Greenland Sea (Faleide et al., 1991). Late Miocene and Pliocene
92 sedimentation, driven by bottom currents, resulted in the formation of the ca. 100 km long Vestnesa Ridge between
93 the HFZ off west-Svalbard and oceanic crust highs at the eastern flank of the Molloy mid-ocean ridge (Eiken and
94 Hinz, 1993; Vogt et al., 1994). The sedimentary ridge is oriented parallel to the Molloy Transform Fault (MTF)
95 and its crest experiences a change in morphology from narrow on the eastern segment to expanded on the western
96 Vestnesa Ridge segment (Fig. 2). The exact location of the continental-ocean boundary remain somewhat uncertain
97 (Eldholm et al., 1987) but it is inferred to be nearby the transition from the eastern to the western segments (Engen
98 et al., 2008).

99

100 The total sedimentary thickness along the Vestnesa Ridge remains unconstrained. Based on one available regional
101 profile it can be inferred that the ridge is > 5 km thick in places (Eiken and Hinz, 1993). It has been divided into
102 three main stratigraphic units (Eiken and Hinz, 1993; Hustoft, 2009): the deepest sequence, YP1, consists of synrift
103 and post-rift sediments deposited directly on oceanic crust; YP2 consists of contourites; and YP3, corresponding
104 to the onset of Pleistocene glaciations (ca. 2.7 Ma ago) (Mattingsdal et al., 2014), is a mix of glaciomarine
105 contourites and turbidites. The effect of ice-sheet dynamics on the west-Svalbard margin (Knies et al., 2009; Patton
106 et al., 2016) has influenced the stratigraphy, and most likely the morphology, of the Vestnesa Ridge and adjacent
107 sedimentary basins. In this Arctic region, glaciations are believed to have started even earlier than 5 Ma ago. The
108 onset of local intensification of glaciations is inferred to have started ca. 2.7 Ma ago (e.g., Faleide et al., 1996;
109 Mattingsdal et al., 2014). Strong climatic fluctuations characterized by intercalating colder, intense glaciations with
110 warmer and longer interglacials, dominated the last ca. 1 Ma. (e.g., Jansen and Sjøholm, 1991; Jansen et al., 1990).

111

112 A set of N-S to NNE-SSE trending faults cut the recent strata at a narrow zone between the Vestnesa Ridge and
113 the northern termination of the KR (Fig 1). Due to their structural connection with the KR they are believed to
114 indicate ongoing northward propagation of the rift system. High resolution 3D seismic data collected on the eastern
115 Vestnesa Ridge segments revealed sub-seafloor NW-SE oriented faults (i.e., near-vertical and parallel to the
116 sedimentary ridge axis) that could be genetically associated with the outcropping faults (Plaza-Faverola et al., 2015;
117 Fig. 2). Comparison of similar high resolution 3D seismic data from the western Vestnesa Ridge segment shows
118 that the style of faulting has been radically different from that of the eastern segment. Here, only randomly oriented
119 small fault segments are revealed in nevertheless pockmarked Holocene strata (Fig. 2). Gravimetric data also

120 indicate an abrupt structural change to the west compared to the east of a N-S oriented fault separating the ridge
121 segments (Plaza-Faverola et al., 2015).

122

123 The gas hydrate system dynamics along the Vestnesa Ridge seems to be highly influenced by spatial variations in
124 the geothermal gradient and the gas composition (Plaza-Faverola et al., 2017). Thermogenic gas accumulations at
125 the base of the GHSZ (Fig. 2) are structurally controlled (i.e., the gas migrates towards the crest of the sedimentary
126 drift) and part of this gas sustains present day seepage activity (Bünz et al., 2012; Knies et al., 2018; Plaza-Faverola
127 et al., 2017). Reservoir modelling shows that source rock deposited north of the MTF has potentially started to
128 generate thermogenic gas 6 Ma ago and that migrating fluids reached the Vestnesa Ridge crest at the active seepage
129 site ca. 2 Ma ago (Knies et al., 2018). It is suspected that seepage has been occurring, episodically, at least since
130 the onset of the Pleistocene glaciations c. 2.7 Ma ago leaving buried pockmarks and authigenic carbonate crusts as
131 footprint (Plaza-Faverola et al., 2015). Many transient seepage events are suspected and one was dated to ca. 17.000
132 years based on the presence of a ~1000 years old methane-dependent bivalve community possibly sustained by a
133 gas pulse through a fault (Ambrose et al., 2015).

134 **3. SEISMIC DATA**

135 The description of faults and fluid flow related features along the Vestnesa Ridge is documented in Plaza-Faverola
136 et al., 2015. The description is based on two-3D high resolution seismic data sets acquired on the western and the
137 eastern Vestnesa Ridge segments respectively, and one 2D seismic line acquired along the entire Vestnesa Ridge
138 extent (Fig. 2 this paper). These data have been previously used for the investigation of BSR dynamics (Plaza-
139 Faverola et al., 2017) and documentation of gas chimneys and faults in the region (Petersen et al., 2010; Plaza-
140 Faverola et al., 2015). The data were acquired on board R/V Helmer Hanssen using the 3D P-Cable system (Planke
141 et al., 2009). Final lateral resolution of the 3D data sets is given by a bin size of 6.25x6.25 m² and the vertical
142 resolution is > 3 m with a dominant frequency of 130 Hz. Details about acquisition and processing can be found in
143 Petersen et al., 2010 and Plaza-Faverola et al., 2015. For the 2D survey the dominant frequency was ~80 Hz
144 resulting in a vertical resolution > 4.5 m (assumed as $\lambda/4$ with an acoustic velocity in water of 1469 m/s given by
145 CTD data; Plaza-Faverola et al., 2017).

146 **4. THE MODELING APPROACH**

147 Tectonic processes at plate margins have a major influence on regional stress patterns (Heidbach et al., 2010).
148 Given the proximity to the Molloy and Knipovich Ridges, we hypothesise that ridge push has a major control on

149 the regional, tectonic stress field at Vestnesa Ridge. Other stress sources of importance in the region may be
150 gravitational stresses due to bathymetry/topography and subsurface density contrasts and flexural stresses due to
151 sediment erosion and deposition. During the Quaternary, the west-Svalbard margin has furthermore been affected
152 by glacially induced flexural stresses due to the glaciations (e.g., Fjeldskaar and Amantov, 2017; Patton et al.,
153 2016). Models of stresses induced by the Fennoscandian ice sheet (Lund et al., 2009; Steffen et al., 2006) indicate
154 that the glacially induced stress on the continental margin is close to zero at present-day.

155

156 This study deals exclusively with tectonic stress due to ridge push. We use the approach by Keiding et al. (2009)
157 based on the analytical solutions derived by Okada (1985), to model the plate motion and tectonic stress field due
158 to spreading along the Molloy and Knipovich Ridges. Because the model only incorporates plate spreading, the
159 stresses resulting from the models cannot be considered as a representation of the total stress field in the region.
160 However, the objective of this study is not to model the total stress field, rather, the focus is to investigate how
161 tectonic stress may influence seepage in the proximity of the two spreading ridges. By excluding all other sources
162 of stress in the modelling, we are able to investigate the influence of plate spreading exclusively.

163

164 The Okada model and our derivation of the stress field from it is described in more detail in appendix A. The
165 Molloy and Knipovich Ridges are modelled as rectangular planes with opening and transform motion in a flat Earth
166 model with elastic, homogeneous, isotropic rheology. Each rectangular plane is defined by ten model parameters
167 used to approximate the location, geometry and deformation of the spreading ridges (Okada, 1985; see supplement
168 Table 1). The locations of the two spreading ridges were constrained from bathymetry maps (Fig. 1). The two
169 spreading ridges are assumed to have continuous, symmetric deformation below the brittle-ductile transition, with
170 a half spreading rate of 7 mm/yr and a spreading direction of N125°E, according to recent plate motion models
171 (DeMets et al., 2010). Because the spreading direction is not perpendicular to the trends of the spreading ridges,
172 this results in both opening and right-lateral motion; that is, oblique spreading on the Molloy and Knipovich Ridges.
173 The Molloy Transform Fault, which connects the two spreading ridges, trends N133°E, thus a spreading direction
174 of N125°E implies extension across the transform zone. We use a depth of 10 km for the brittle-ductile transition
175 and 900 km for the lower boundary of the deforming planes, to avoid boundary effects. For the elastic rheology,
176 we assume typical crustal values of Poisson's ratio = 0.25 and shear modulus = 30 GPa (Turcotte and Schubert,
177 2002).

178 Asymmetric spreading has been postulated for the Knipovich Ridge based on heat flow data (Crane et al., 1991),
179 and for other ultraslow spreading ridges based on magnetic data (e.g., Gaina et al., 2015). However, the evidence

180 for asymmetry along the KR remains inconclusive and debatable in terms, for example, of the relative speeds
181 suggested for the North American (faster) and the Eurasian (slower) plates (Crane et al., 1991; Morgan, 1981; Vogt
182 et al., 1994). This reflects that the currently available magnetic data from the west-Svalbard margin is not of a
183 quality that allows an assessment of possible asymmetry of the spreading in the Fram Strait (Nasuti and Olesen,
184 2014). Thus, symmetry is conveniently assumed for the purpose of the present study.

185

186 We focus on the stress field in the upper part of the crust (where the GHSZ is) and characterise the stress regime
187 based on the relative magnitudes of the horizontal and vertical stresses. We refer to the stresses as σ_v (vertical
188 stress), σ_H (maximum horizontal stress) and σ_h (minimum horizontal stress), where compressive stress is positive
189 (Zoback and Zoback, 2002). A tensile stress regime ($\sigma_v > \sigma_H > \sigma_h$) favours the opening of steep faults that can
190 provide pathways for fluids. Favourable orientation of stresses with respect to existing faults and/or pore fluid
191 pressures increasing beyond hydrostatic pressures are additional conditions for leading to opening for fluids under
192 strike-slip ($\sigma_H > \sigma_v > \sigma_h$) and compressive ($\sigma_H > \sigma_h > \sigma_v$) regimes (e.g., Grauls and Baleix, 1994).

193

194 **4. RESULTS AND DISCUSSION**

195 **4.1 PREDICTED STRESS FIELDS DUE TO OBLIQUE SPREADING**

196

197 The model predicts zones of tensile stress near the spreading ridges, and strike-slip at larger distance from the
198 ridges. An unexpected pattern arises near the Vestnesa Ridge due to the interference of the stress from the two
199 spreading ridges. A zone of tensile stress extends northward from the Knipovich Ridge, encompassing the eastern
200 part of the Vestnesa Ridge. The western Vestnesa Ridge, on the other hand, lies entirely in a zone of strike-slip
201 stress (Fig. 4).

202

203 Sensitivity tests for realistic variations in 1) mid-oceanic spreading, 2) depth of the brittle-ductile transition, and 3)
204 elastic moduli, show that the tensile stress zone covering the eastern Vestnesa Ridge is a robust feature of the
205 model, that is, variations in the parameters result in a change of the extent and shape of the tensile zone but the
206 zone remains in place (Supplementary material).

207

208 To investigate the geometric relationship between the predicted stress field and mapped faults, we calculate the
209 orientations of maximum compressive horizontal stress (Lund and Townend, 2007) . The maximum horizontal
210 stresses (σ_H) within the tensile regime approximately follow the orientation of the spreading axes (i.e., dominantly

211 NE-SW to N-S; Fig. 4). Spreading along the Molloy ridge causes NW-SE orientation of the maximum compressive
212 stress along most of the Vestnesa Ridge, except for the eastern segment where the influence of the Knipovich Ridge
213 results in a rotation of the stress towards E-W (Fig. 4). It is important to wear in mind that the minimum horizontal
214 compressive stresses (σ_h) would be exerted in a plane perpendicular to the vectors in figure 4 (see Fig. 2).

215

216 The simplifying assumptions involved in the Okada models (e.g., continuous, symmetric deformation below the
217 brittle-ductile transition) implies that the resulting stresses are unconstrained to a certain degree. However,
218 Árnadóttir et al. (2009) demonstrated that the deformation field from the complex plate boundary in Iceland could
219 be modelled using Okada models. In addition, the predicted stress directions from Okada models are in general
220 agreement with other models of plate tectonic forces (e.g., Gölke & Coblenz, 1996; Naliboff et al., 2012).
221 Furthermore, a comparison of the predicted stress from plate spreading and observed earthquake focal mechanisms
222 shows an excellent agreement, both with regards to style and orientation of the focal mechanisms. The earthquake
223 focal mechanisms are mostly normal along the spreading ridges and strike-slip along the transform faults, and the
224 focal mechanism pressure axes align nicely with the predicted directions of maximum compressive stress (Fig. 4).
225 The good agreement between Okada's and other modelling approaches as well as between the resulting stresses
226 and focal mechanisms in the area indicates two things: 1. that the model, despite the simplicity of its assumptions,
227 provides a correct first order prediction of the stress field in the upper crust, and 2. that stress from plate spreading
228 may indeed have a dominant control on the stress field along the Vestnesa Ridge.

229

230 **4.2 SPATIAL CORRELATION BETWEEN MODELLED TECTONIC STRESS REGIME, FAULTING** 231 **AND FLUID FLOW FEATURES**

232

233 The zone of tensile stress on the eastern Vestnesa Ridge segment coincides with a zone of faulting and where all
234 the present day seepage is concentrated (Fig. 3, 4). The match between the extent of the modelled tensile zone and
235 the active pockmarks is not exact; active pockmarks exist a few kilometres westward from the termination of the
236 tensile zone (Fig. 4). However, the agreement is striking from a regional point of view, considering the uncertainty
237 of the model as illustrated by the sensitivity tests (Supplementary material). In the predicted tensile zone towards
238 the east of the Vestnesa Ridge, the sub-seabed faults are NW-SE oriented, near vertical and have a gentle normal
239 throw (< 10 m). Normal faulting or tensile opening of these faults would be enhanced by NW-SE oriented
240 maximum compressive stress, i.e., the orientation of stresses predicted by our model on the crest and at the southern
241 flank of the ridge until the transition to the tensile stress regime (Fig. 4). This implies that these faults are currently

242 under a regime that makes them favourably permeable for fluids (Fig. 2). Indeed, these faults are spatially linked
243 to gas chimneys and active seepage (Bünz et al., 2012; Plaza-Faverola et al., 2015). Some of the faults show thicker
244 sediment thicknesses at the hanging wall, allowing identification of discrete periods of normal faulting (Plaza-
245 Faverola et al., 2015).

246

247 The character of the faults changes towards the western Vestnesa Ridge where the model predicts a strike-slip
248 regime (Fig. 2). The density of faulting and seismic definition decreases westward (Fig. 2, 3, 5). In this part of the
249 ridge gas chimneys are narrower, stacked more vertically than active chimneys towards the east and it is possible
250 to recognise more faults reaching the present-day seafloor (Plaza-Faverola et al., 2015). Here, the orientation of σ_H
251 (NW-SE) is oblique to the more WNW-ESE to W-E oriented fault segments (Fig. 2, 4), suggesting that, with some
252 exceptions, these structures are less favourably oriented for tensile opening than the structures imaged towards the
253 east (Fig. 2).

254

255 The cluster of larger scale N-S to NNW-SSE trending extensional faults that outcrop at the southern slope of the
256 Vestnesa Ridge (Fig. 1, 2), also coincides with the zone of predicted tensile stress (Fig. 4). In agreement with our
257 models, these extensional faults have been suggested to indicate the northward propagation of the Knipovich Ridge
258 rift system (Crane et al., 2001; Vanneste et al., 2005). However, it is likely that faulting along this steep slope of
259 the Vestnesa Ridge (Fig. 1) was partially induced as well by gravitational stress.

260

261 The striking correlation between predicted tectonic stress regime, faulting structures and current seepage suggests
262 that tectonic stress resulting from oblique spreading in the region, has potentially a major influence on the near-
263 surface sedimentary deformation and fluid dynamics. Hereafter, we discuss the implications of the interaction
264 between tectonic stresses and pore-fluid pressure for the evolution of gas seepage along the Vestnesa Ridge.

265

266 **4.3 SEEPAGE COUPLED TO STRESS CYCLING**

267 Based on the correlation between tectonic stress regimes and seepage patterns, we postulate that current seepage at
268 the eastern Vestnesa Ridge segment is favoured by the opening of pre-existing faults in a tensile stress regime (Fig.
269 2, 3b). Depending on the tectonic regime, permeability through faults and fractures may be enhanced or inhibited
270 (e.g., Faulkner et al., 2010; Hillis, 2001; Sibson, 1994). Thus, spatial and temporal variations in the tectonic stress
271 regime may control the transient release of gas from the seafloor over geological time as documented, for example,
272 for CO₂ analogues in the Colorado Plateau (e.g., Jung et al., 2014).

273

274 It is likely that the steep NW-SE oriented faults mapped along the eastern Vestnesa Ridge segment formed in a
275 strike-slip regime and became permeable to fluids over time. We envision that seepage is induced 1) by opening of
276 faults favourably oriented with respect to the stress field and 2) by high pore fluid pressure at the base of the GHSZ
277 (i.e., the shallowest reservoir holding gas from escaping to the seafloor). Thus, seepage along the Vestnesa Ridge
278 may have been driven by cyclic changes in stress or pore fluid pressure. Opening of fractures is facilitated if the
279 minimum horizontal stress is smaller than the pore-fluid pressure (p_f), that is, the minimum effective stress is
280 negative ($\sigma_h' = \sigma_h - p_f < 0$) (e.g., Grauls and Baleix, 1994). Secondary permeability may increase by formation of
281 tension fractures near damaged fault zones (Faulkner et al., 2010). A negative minimum effective stress and
282 subsequent increase in secondary permeability in a tensile stress regime can be achieved particularly easy in the
283 near-surface. Continued flow through opened faults and fractures would explain brecciation and development of
284 the observed chimneys (Fig. 2b) (e.g., Sibson, 1994).

285

286 Seepage through gas chimneys has been dominantly advective and episodic (Fig. 2; Plaza-Faverola et al., 2005)
287 likely due to consecutive decreases and increases in the pore fluid pressure at the base of the GHSZ in response to
288 both, regional stress field variations and also to local pressure alterations associated for example with
289 hydrofracturing (e.g., Hustoft et al., 2010 and references therein; Karstens and Berndt, 2015). Pressure increases at
290 the base of the GHSZ in this part of the ridge is explained by a constant input of thermogenic gas from an Eocene
291 reservoir since at least ca. 2 Ma ago (Knies et al., 2018).

292

293 The fact that there is not active seepage at present along the western Vestnesa Ridge segment (i.e., being under a
294 strike-slip regime according to the models) is interesting, and somehow supports the notion that the tensile regime
295 affects the fluid flow system towards the eastern segment. The lack of seepage at present in the western segment
296 suggests that p_f at the base of the GHSZ is not high enough to overcome the minimum horizontal stress (i.e., σ_h' is
297 positive) (Fig. 3a).

298

299 **4.4 PAST SEEPAGE – AN EFFECT OF GLACIAL STRESSES?**

300

301 While tectonic stresses are constant over short geological time spans, chimney development and seafloor seepage
302 has been a transient process because of slight variations in pore-fluid pressure (as discussed above) or the influence
303 of other stress generating mechanisms that have repeatedly brought the system out of equilibrium. Geophysical and

304 paleontological data indicate that there was once seepage and active chimney development on the western Vestnesa
305 Ridge segment (e.g., Consolaro et al., 2015; Plaza-Faverola et al., 2015; Schneider et al., 2018).
306

307 Following the same logic as for the present day seepage explanation, the negative σ_h' condition could have been
308 attained anywhere along the Vestnesa Ridge in the past due to pore fluid pressure increases at the base of the GHSZ
309 or due to a favourable orientation of the stress regime at the time. Until now, we have just discussed the potential
310 effect on seepage exerted by stresses resulting exclusively from oblique spreading at the mid-ocean ridges.
311 However, and as indicated in previous sections, glacial isostasy is potentially other important historical source of
312 stress influencing the total stress field in the region (e.g., Lund et al., 2009) . During glacial periods, the load of the
313 ice forces the lithosphere down and creates a forebulge along the periphery of the ice, resulting in flexural stresses
314 in the upper part of the lithosphere (Lund and Schmidt, 2011). The lateral expansion of grounded ice in the western
315 Barents Sea region is limited by the continental shelf break (Fig. 1), thus the Vestnesa Ridge may have been located
316 within the isostatic forebulge at given periods of times during the glaciations (Patton et al., 2016).
317

318 We cannot conclusively argue about the potential effect of tensile stresses from current glacial isostasy over the
319 Vestnesa Ridge at present. However, by simple analogy with the kind of compressive stresses (magnitude and
320 orientation) reported beyond the shelf break off the mid-Norwegian margin for time spans close to present day ice
321 condition, we can sense that such an effect is minimal at present (Lund and Schmidt, 2011; Lund et al., 2009). In
322 general, it is expected that maximum glacially induced horizontal stresses (σ_H) would be dominantly oriented
323 parallel to the shelf break (Björn Lund personal communication; Lund et al., 2009). This is, dominantly N-S in the
324 area of the Vestnesa Ridge (Fig. 1). Such stress orientation would not favour opening for fluids along pre-existing
325 NW-SE oriented faults associated with seepage activity at present (i.e., N-S oriented faults would be the more
326 vulnerable for opening). It is likely, though, that the repeated waxing and waning of the ice sheet caused a cyclic
327 modulation of the stress field (varying magnitude and orientation) and influenced the dynamics of gas
328 accumulations and favourably oriented faults along the Vestnesa Ridge in the past. Past glacial stresses may provide
329 thus an alternative explanation for seepage along the entire Vestnesa Ridge extent at given periods of time (Fig. 5);
330 in line with the correlation between seepage and glacial-interglacial events postulated for different continental
331 margins e.g., for chimneys off the mid-Norwegian margin (Plaza-Faverola et al., 2011), the Gulf of Lion (Riboulot
332 et al., 2014), but also along the Vestnesa Ridge (Plaza-Faverola et al., 2015; Schneider et al., 2018).
333

334 The temporal variation in the stress field along the Vestnesa Ridge is also caused by its location on a constantly
335 growing plate. As the oceanic plate grows, the Vestnesa Ridge moves eastward with respect to the Molloy and
336 Knipovich Ridges, causing a westward shift in the regional stress field on the Vestnesa Ridge (Fig. 6). In the future,
337 the eastern Vestnesa Ridge may temporarily move out of the tensile zone, while the western Vestnesa Ridge moves
338 into it (Fig. 6). This suggests that a negative effective stress and subsequent active seepage may reappear at
339 pockmarks to the west of the currently active seepage zone.

340

341 The effect of glacial stresses over the fluid flow system off west-Svalbard will be further tested (at least for the
342 Weichselian period) by implementing Lund et al., models using newly constrained Barents Sea ice-sheet models
343 (Patton et al., 2016). Additional sources of stress related to topography/bathymetry should be further investigated
344 as well to gain a comprehensive assessment of the effect of the total stress field on near-surface fluid migration in
345 the region.

346

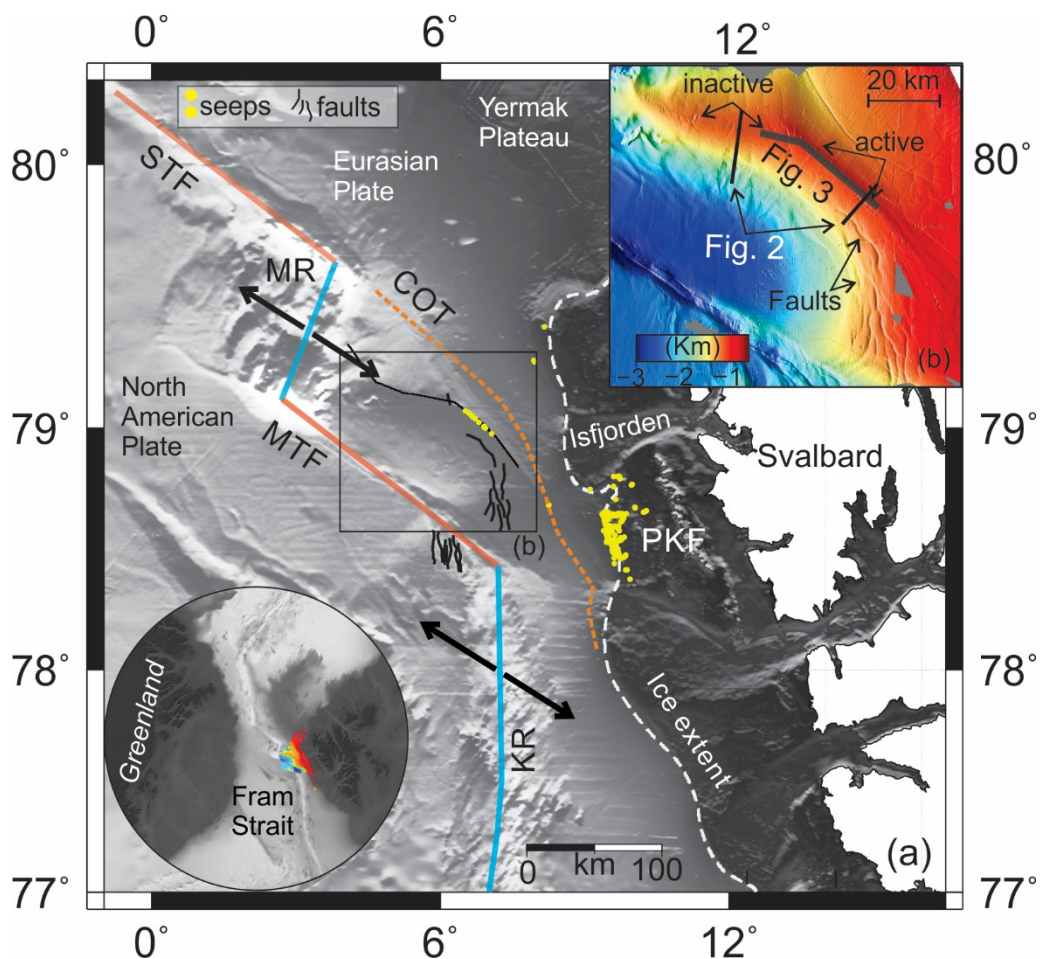
347 **6- CONCLUSIONS**

348

349 The results of modelling the stress regime generated exclusively by mid-ocean ridge spreading in the Fram Strait
350 support seismic evidence of the correlation between faulting and seepage distribution along the Vestnesa
351 sedimentary ridge, offshore the west Svalbard margin. Tectonic stresses due to oblique spreading along the Molloy
352 and the Knipovich ridges influences the present-day stress field across the west-Svalbard passive margin. A
353 correlation between a tensile stress regimes and seepage activity suggests that episodic seepage through gas
354 chimneys has been controlled by an interplay between varying minimum horizontal stresses and pore fluid pressure
355 at the free gas zone beneath the gas hydrate reservoir. Our study suggests that present-day seepage is facilitated by
356 opening of faults and fractures in a tensile stress regime or dilation on faults favourably oriented in a strike-slip
357 regime, where pore fluid pressure overcomes the minimum horizontal stress. Multiple seepage events along the
358 entire extent of the Vestnesa Ridge, may have been triggered either by favourable orientation of faults with respect
359 to mid-ocean ridge derived-stresses in the past or by additional sources of stress related for example to glacial
360 isostasy. Future reactivation of currently dormant pockmarks is likely following the gradual westward propagation
361 of the tensile stress zone on the Vestnesa Ridge as the Eurasian plate drift towards the south-east.

362

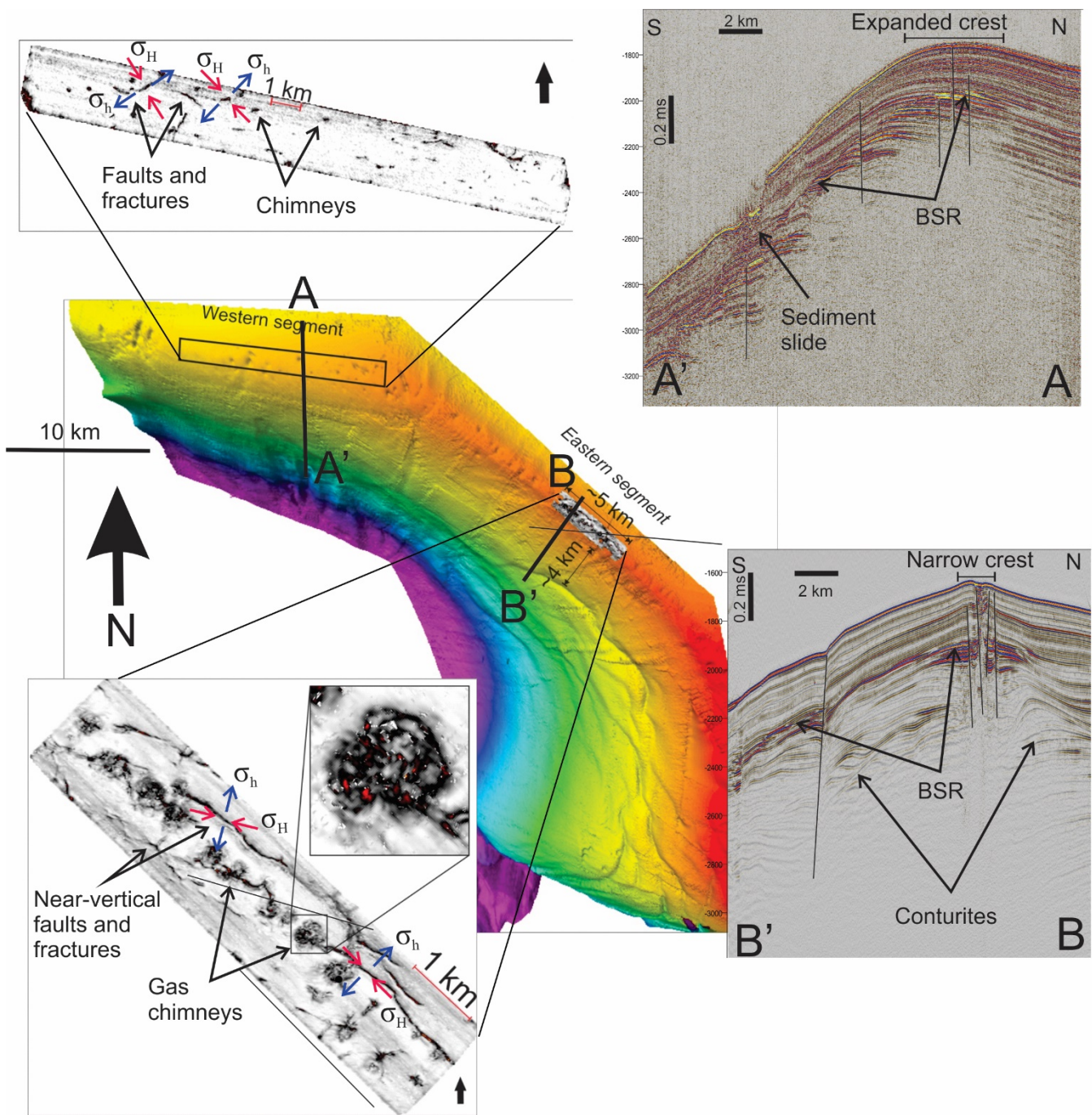
363 **Figures**



364
 365 **Figure 1:** (a) International Bathymetry Chart of the Arctic Ocean (IBCAO) showing the geometry of mid-ocean
 366 ridges offshore the west-Svalbard margin; (b) High resolution bathymetry along the Vestnesa Ridge (UiT, R/V HH
 367 multi-beam system). Seafloor pockmarks are observed along the entire ridge but active seep sites are restricted to
 368 its eastern segment; PKF=Prins Karl Foreland; STF=Spitsbergen Transform Fault; MR=Molloy Ridge;
 369 MTF=Molloy Transform Fault; KR=Knipovich Ridge; COT=Continental-Oceanic Transition (Engen et al., 2008);
 370 Ice-Sheet Extent (Patton et al., 2016).

371

372

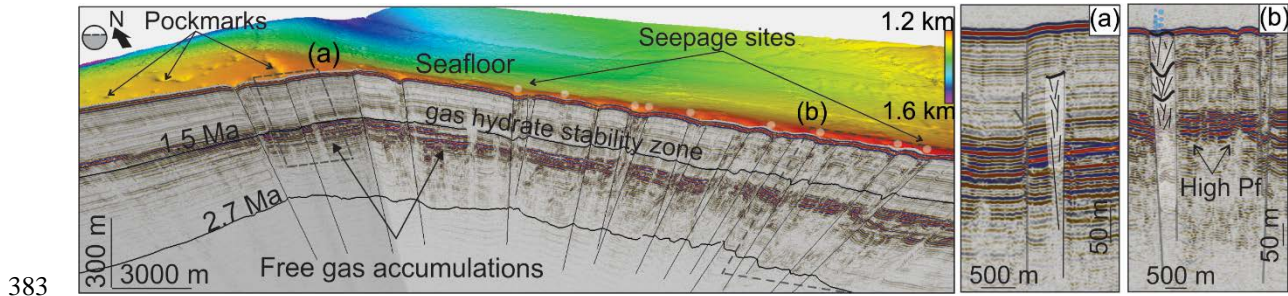


373
374

375 Figure 2: Composite figure with bathymetry and variance maps from 3D seismic data along the eastern and the
376 western Vestnesa Ridge segments (modified from Plaza-Faverola et al., 2015). The orientation of maximum

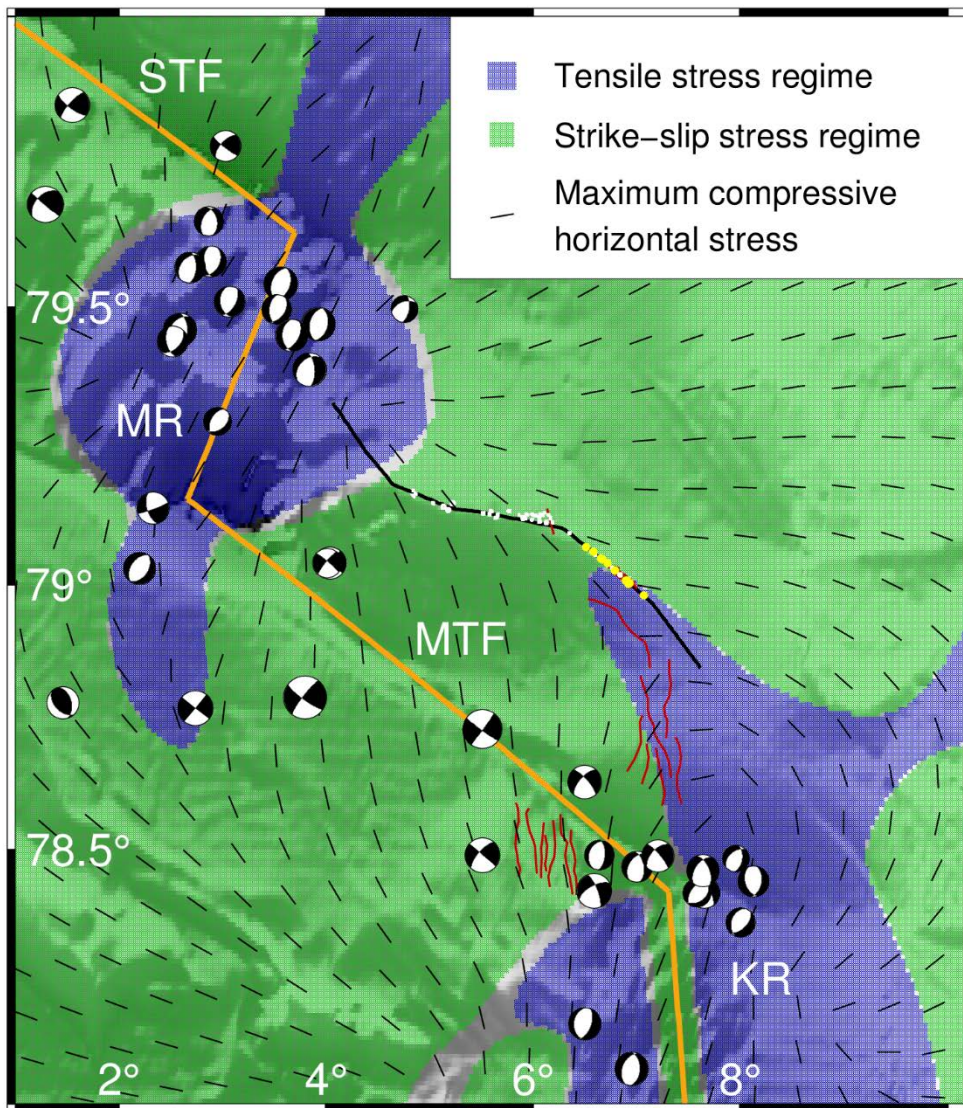
377 compressive horizontal stress (σ_H) and minimum horizontal stress (σ_h) predicted by the model are projected over
378 selected fault segments. Notice favourable orientation for opening to fluids on the eastern Vestnesa Ridge segment.
379 Two-2D seismic transects (A-A' - Büinz et al., 2012 and B-B' – Johnson et al., 2015) illustrate the morphological
380 difference of the crest of the Vestnesa Ridge (i.e., narrow vs. extended) believed to be determined by bottom current
381 dominated deposition and erosion (Eiken and Hinz, 1993).

382



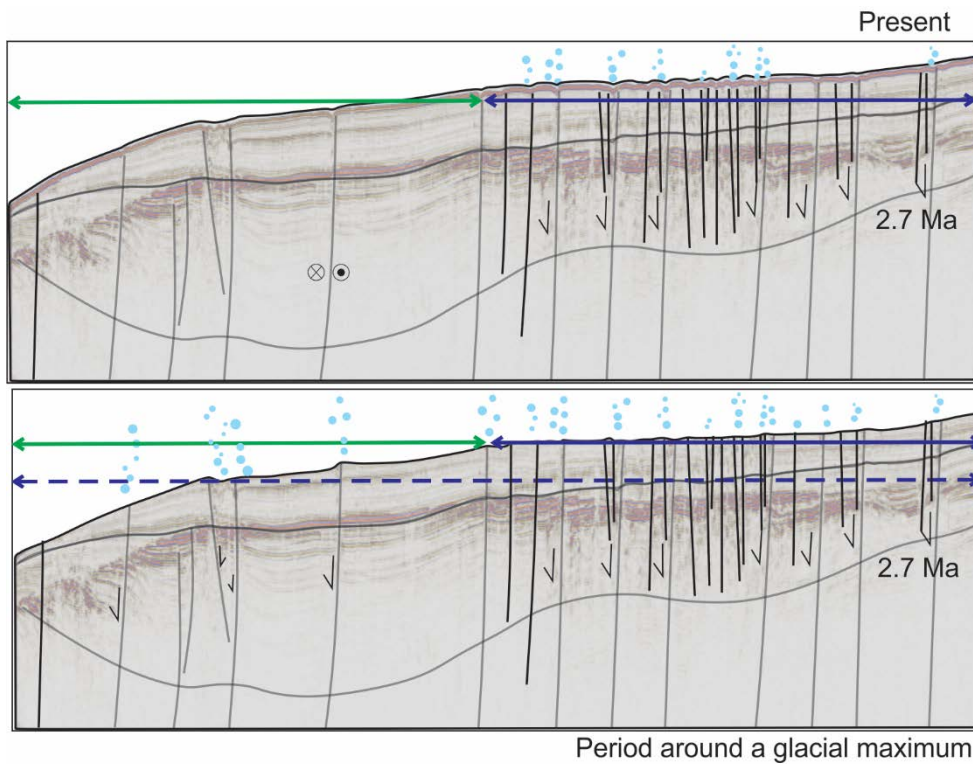
384 **Figure 3:** Integrated seismic and bathymetry image of the gas hydrate system along the Vestnesa Ridge. (a)
385 Outcropping fault located at the transition from the active to the currently inactive pockmark region; (b) Gas
386 chimneys with active seepage and inferred high pore-fluid pressure (Pf) zone.

387



388

389 **Figure 4:** Modelled upper crustal tectonic stress field (blue – tensile and green - strike-slip regime) and stress
 390 orientations, due to oblique spreading at Molloy Ridge (MR) and Knipovich Ridge (KR). The seismic line is
 391 projected as reference for the crest of the Vestnesa Ridge. Red lines are faults, yellow dots seeps and white circles
 392 inactive pockmarks. The focal mechanisms are from the ISC Online Bulletin (<http://www.isc.ac.uk>).



Period around a glacial maximum

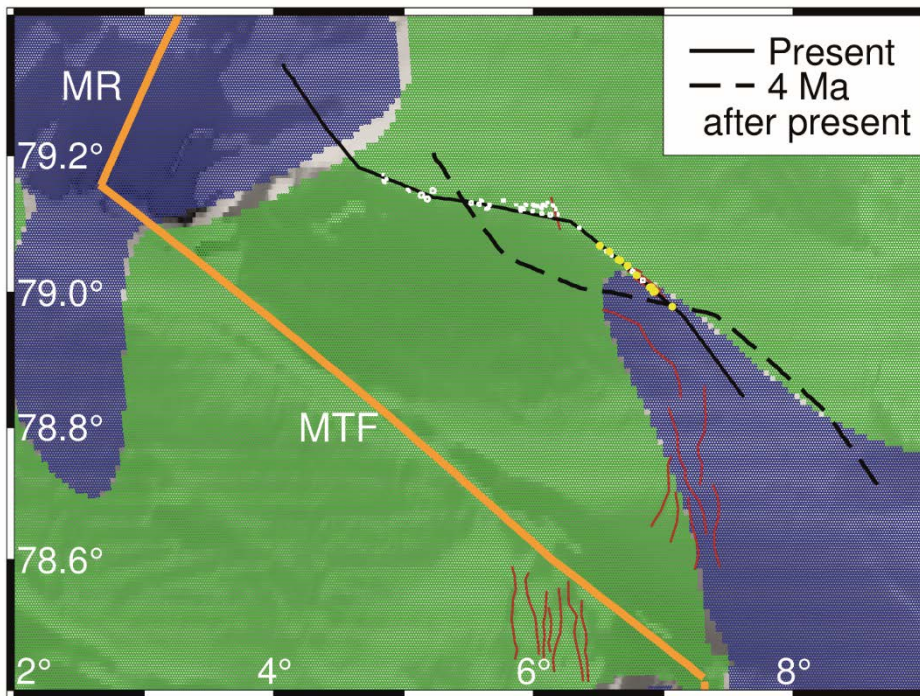
393

394 **Figure 5:** Conceptual model of the evolution of seepage coupled to faulting and spatial variations in the stress
 395 regime (tensile=blue; strike-slip=green) along the Vestnesa Ridge, offshore the west-Svalbard margin. At present
 396 day, tensile stress from mid-ocean ridge spreading (blue solid line) favours seepage exclusively on the eastern
 397 segment of the Vestnesa Ridge. Seepage on the western Vestnesa Ridge and other regions may have been induced
 398 repeatedly since the onset of glaciations 2.7 Ma ago (Mattingsdal et al., 2014), due to tensional flexural stresses in
 399 the isostatic forebulge around the time of glacial maximums.

400

401

402



403

404 **Figure 6:** Stress field in figure 3 showing the location of the Vestnesa Ridge at present and 4 Ma after present time,
 405 assuming a constant spreading velocity of 7 mm/yr in the direction N125°E. The black polygon corresponds to the
 406 seismic line in Plaza-Faverola et al., 2017 and partly shown in figure 3. It is presented as reference for the crest of
 407 the eastern and western Vestnesa Ridge segments

408

409 **Appendix A**

410 **Model description**

411

412 We use the analytical formulations of Okada (1985) for a finite rectangular dislocation source in elastic
 413 homogeneous isotropic half-space (Fig. A.1). The dislocation source can be used to approximate deformation along
 414 planar surfaces, such as volcanic dykes (e.g. Wright et al., 2006), sills (e.g. Pedersen and Sigmundsson, 2004),
 415 faults (e.g. Massonet et al, 1993) and spreading ridges (e.g. Keiding et al., 2009). More than one dislocations can
 416 be combined to obtain more complex geometry of the source or varying deformation along a planar source. The
 417 deformation of the source can be defined as either lateral shear (strike-slip for faults), vertical shear (dip-slip at
 418 faults) or tensile opening.

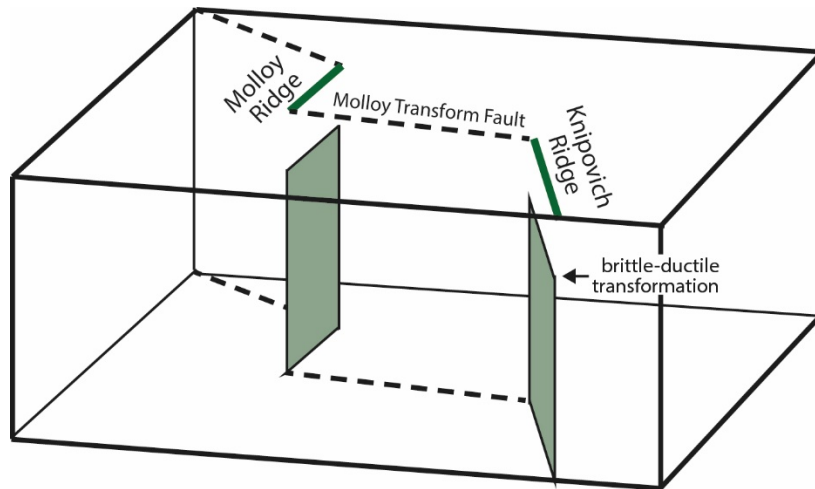
419

420 The Okada model assumes flat Earth without inhomogeneities. While the flat-earth assumption is usually adequate
 421 for regional studies (e.g. Wolf, 1984), the lateral inhomogeneities can sometimes cause considerable effect on the
 422 deformation field (e.g. Okada, 1985). However, the dislocation model is useful as a first approximation to the
 423 problem.

424

425 At mid-ocean ridges, deformation is driven by the continuous spreading caused primarily by gravitational stress
 426 due to the elevation of the ridges, but also basal drag and possibly slab pull. Deformation occurs continuously in
 427 the ductile part of the crust. Meanwhile, elastic strain builds in the upper, brittle part of the crust. To model this
 428 setting, the upper boundary of the dislocation source must be located at the depth of the brittle-ductile transition
 429 zone. The lower boundary of the source is set to some arbitrary large depth to avoid boundary effects.

430



431

432 **Fig A.1 Extract of model showing the location of the dislocation sources (light green) for Molloy and**
 433 **Knipovich ridges. Note that the model is an infinite half-space, i.e. it has no lateral or lower boundary.**

434

435 The Okada model provides the displacements u_x, u_y, u_z (or velocities if deformation is time-dependent) at defined
 436 grid points at the surface and subsurface. It also provides strain (or strain rates) defined as:

437

$$\varepsilon_{ij} = \frac{1}{2}(u_{i,j} + u_{j,i})$$

438 The stress field can then be calculated from the predicted strain rates. In homogeneous isotropic media, stress is
 439 related to strain as:

440

$$\sigma_{ij} = \lambda \delta_{ij} \varepsilon_{kk} + 2\mu \varepsilon_{ij}$$

441 where δ_{ij} if the Kronecker delta, λ is Lamé's first parameter, and μ is the shear modulus. Lamé's first parameter
442 does not have a physical meaning but is related to the shear modulus and Poisson's ratio (ν) as $\lambda = \frac{2\mu\nu}{1-2\nu}$.
443 The absolute values of stress are in general difficult to model (e.g. Hergert and Heidbach, 2011), and not possible
444 with our analytical model. However, the model provides us with the orientations and relative magnitude of the
445 stresses. That is, we know the relative magnitudes of the vertical stress (σ_v), maximum horizontal stress (σ_H) and
446 minimum horizontal stress (σ_h). From this, the stress regime can be defined as either tensile ($\sigma_v > \sigma_H > \sigma_h$), strike-
447 slip ($\sigma_H > \sigma_v > \sigma_h$) or compressive ($\sigma_H > \sigma_h > \sigma_v$).

448

449 **Author contribution**

450 Andreia Plaza-Faverola conceived the paper idea. She is responsible for seismic data processing and interpretation.
451 Marie Keiding did the tectonic modelling. The paper is the result of integrated work between both.

452

453 **ACKNOWLEDGEMENTS**

454 This research is part of the Centre for Arctic Gas Hydrate, Environment and Climate (CAGE) supported by the
455 Research Council of Norway through its Centres of Excellence funding scheme grant No. 223259. Marie Keiding
456 is supported by the NEONOR2 project at the Geological Survey of Norway. Special thanks to Björn Lund, Peter
457 Schmidt, Henry Patton, and Alun Hubbard for their interest in the present project and constructive discussions
458 about isostasy and glacial stresses. We are thankful to various reviewers that have contributed to the improvement
459 of the manuscript. Seismic data is archived at CAGE – Centre for Arctic Gas Hydrate, Environment and Climate,
460 Tromsø, Norway and can be made available by contacting APF. Modelled stresses can be made available by
461 contacting MK.

462

463 **References:**

464 Ambrose, W.G., Panieri, G., Schneider, A., Plaza-Faverola, A., Carroll, M.L., Åström, E.K., Locke, W.L.,
465 Carroll, J., 2015. Bivalve shell horizons in seafloor pockmarks of the last glacial-interglacial transition: a
466 thousand years of methane emissions in the Arctic Ocean. *Geochemistry, Geophysics, Geosystems* 16, 4108-
467 4129.
468 Andreassen, K., Hubbard, A., Winsborrow, M., Patton, H., Vadakkepuliambatta, S., Plaza-Faverola, A.,
469 Gudlaugsson, E., Serov, P., Deryabin, A., Mattingdal, R., 2017. Massive blow-out craters formed by hydrate-
470 controlled methane expulsion from the Arctic seafloor. *Science* 356, 948-953.
471 Árnadóttir, T., Lund, B., Jiang, W., Geirsson, H., Björnsson, H., Einarsson, P., Sigurdsson, T., 2009. Glacial
472 rebound and plate spreading: results from the first countrywide GPS observations in Iceland. *Geophysical Journal*
473 *International* 177, 691-716.

474 Bünz, S., Polyanov, S., Vadakkepuliambatta, S., Consolaro, C., Mienert, J., 2012. Active gas venting through
475 hydrate-bearing sediments on the Vestnesa Ridge, offshore W-Svalbard. *Marine geology*.

476 Consolaro, C., Rasmussen, T., Panieri, G., Mienert, J., Bünz, S., Szybor, K., 2015. Carbon isotope ($\delta^{13}\text{C}$)
477 excursions suggest times of major methane release during the last 14 kyr in Fram Strait, the deep-water gateway
478 to the Arctic. *Climate of the Past* 11, 669-685.

479 Crane, K., Doss, H., Vogt, P., Sundvor, E., Cherkashov, G., Poroshina, I., Joseph, D., 2001. The role of the
480 Spitsbergen shear zone in determining morphology, segmentation and evolution of the Knipovich Ridge. *Marine*
481 *geophysical researches* 22, 153-205.

482 Crane, K., Sundvor, E., Buck, R., Martinez, F., 1991. Rifting in the northern Norwegian-Greenland Sea: Thermal
483 tests of asymmetric spreading. *Journal of Geophysical Research: Solid Earth* 96, 14529-14550.

484 DeMets, C., Gordon, R.G., Argus, D.F., 2010. Geologically current plate motions. *Geophysical Journal*
485 *International* 181, 1-80.

486 Dickens, G.R., 2011. Down the rabbit hole: Toward appropriate discussion of methane release from gas hydrate
487 systems during the Paleocene-Eocene thermal maximum and other past hyperthermal events. *Climate of the Past*
488 7, 831-846.

489 Ehlers, B.-M., Jokat, W., 2009. Subsidence and crustal roughness of ultra-slow spreading ridges in the northern
490 North Atlantic and the Arctic Ocean. *Geophysical Journal International* 177, 451-462.

491 Eiken, O., Hinz, K., 1993. Contourites in the Fram Strait. *Sedimentary Geology* 82, 15-32.

492 Eldholm, O., Faleide, J.I., Myhre, A.M., 1987. Continent-ocean transition at the western Barents Sea/Svalbard
493 continental margin. *Geology* 15, 1118-1122.

494 Engen, Ø., Faleide, J.I., Dyreng, T.K., 2008. Opening of the Fram Strait gateway: A review of plate tectonic
495 constraints. *Tectonophysics* 450, 51-69.

496 Faleide, J., Gudlaugsson, S., Eldholm, O., Myhre, A., Jackson, H., 1991. Deep seismic transects across the
497 sheared western Barents Sea-Svalbard continental margin. *Tectonophysics* 189, 73-89.

498 Faleide, J.I., Solheim, A., Fiedler, A., Hjelstuen, B.O., Andersen, E.S., Vanneste, K., 1996. Late Cenozoic
499 evolution of the western Barents Sea-Svalbard continental margin. *Global and Planetary Change* 12, 53-74.

500 Faulkner, D., Jackson, C., Lunn, R., Schlische, R., Shipton, Z., Wibberley, C., Withjack, M., 2010. A review of
501 recent developments concerning the structure, mechanics and fluid flow properties of fault zones. *Journal of*
502 *Structural Geology* 32, 1557-1575.

503 Fjeldskaar, W., Amantov, A., 2017. Effects of glaciations on sedimentary basins. *Journal of Geodynamics*.

504 Gaina, C., Nikishin, A., Petrov, E., 2015. Ultraslow spreading, ridge relocation and compressional events in the
505 East Arctic region: A link to the Eurekan orogeny? *arktos* 1, 16.

506 Geersen, J., Scholz, F., Linke, P., Schmidt, M., Lange, D., Behrmann, J.H., Völker, D., Hensen, C., 2016. Fault
507 zone controlled seafloor methane seepage in the rupture area of the 2010 Maule Earthquake, Central Chile.
508 *Geochemistry, Geophysics, Geosystems* 17, 4802-4813.

509 Grauls, D., Baleix, J., 1994. Role of overpressures and in situ stresses in fault-controlled hydrocarbon migration:
510 A case study. *Marine and Petroleum Geology* 11, 734-742.

511 Gölke, M., Coblentz, D., 1996. Origins of the European regional stress field. *Tectonophysics* 266, 11-24.

512 Heidbach, O., Tingay, M., Barth, A., Reinecker, J., Kurfeß, D., Müller, B., 2010. Global crustal stress pattern
513 based on the World Stress Map database release 2008. *Tectonophysics* 482, 3-15.

514 Hillis, R.R., 2001. Coupled changes in pore pressure and stress in oil fields and sedimentary basins. *Petroleum*
515 *Geoscience* 7, 419-425.

516 Hunter, S., Goldobin, D., Haywood, A., Ridgwell, A., Rees, J., 2013. Sensitivity of the global submarine hydrate
517 inventory to scenarios of future climate change. *Earth and Planetary Science Letters* 367, 105-115.

518 Hustoft, S., Bunz, S., Mienert, J., Chand, S., 2009. Gas hydrate reservoir and active methane-venting province in
519 sediments on < 20 Ma young oceanic crust in the Fram Strait, offshore NW-Svalbard. *Earth and Planetary*
520 *Science Letters* 284, 12-24.

521 Hustoft, S., Bünz, S., Mienert, J., 2010. Three-dimensional seismic analysis of the morphology and spatial
522 distribution of chimneys beneath the Nyegga pockmark field, offshore mid-Norway. *Basin Research* 22, 465-480.

523 Jakobsson, M., Backman, J., Rudels, B., Nycander, J., Frank, M., Mayer, L., Jokat, W., Sangiorgi, F., O'Regan,
524 M., Brinkhuis, H., 2007. The early Miocene onset of a ventilated circulation regime in the Arctic Ocean. *Nature*
525 447, 986-990.

526 Jansen, E., Sjøholm, J., 1991. Reconstruction of glaciation over the past 6 Myr from ice-borne deposits in the
527 Norwegian Sea. *Nature* 349, 600.

528 Jansen, E., Sjøholm, J., Bleil, U., Erichsen, J., 1990. Neogene and Pleistocene glaciations in the northern
529 hemisphere and late Miocene—Pliocene global ice volume fluctuations: Evidence from the Norwegian Sea,
530 *Geological History of the Polar Oceans: Arctic versus Antarctic*. Springer, pp. 677-705.

531 Johnson, J.E., Mienert, J., Plaza-Faverola, A., Vadakkepuliambatta, S., Knies, J., Bünz, S., Andreassen, K.,
532 Ferré, B., 2015. Abiotic methane from ultraslow-spreading ridges can charge Arctic gas hydrates. *Geology*,
533 G36440. 36441.

534 Judd, A., Hovland, M., 2009. *Seabed fluid flow: the impact on geology, biology and the marine environment*.
535 Cambridge University Press.

536 Jung, N.-H., Han, W.S., Watson, Z., Graham, J.P., Kim, K.-Y., 2014. Fault-controlled CO₂ leakage from natural
537 reservoirs in the Colorado Plateau, East-Central Utah. *Earth and Planetary Science Letters* 403, 358-367.

538 Karstens, J., Berndt, C., 2015. Seismic chimneys in the Southern Viking Graben—Implications for palaeo fluid
539 migration and overpressure evolution. *Earth and Planetary Science Letters* 412, 88-100.

540 Keiding, M., Lund, B., Árnadóttir, T., 2009. Earthquakes, stress, and strain along an obliquely divergent plate
541 boundary: Reykjanes Peninsula, southwest Iceland. *Journal of Geophysical Research: Solid Earth* 114.

542 Knies, J., Daszinnies, M., Plaza-Faverola, A., Chand, S., Sylta, Ø., Bünz, S., Johnson, J.E., Mattingsdal, R.,
543 Mienert, J., 2018. Modelling persistent methane seepage offshore western Svalbard since early Pleistocene.
544 *Marine and Petroleum Geology* 91, 800-811.

545 Knies, J., Matthiessen, J., Vogt, C., Laberg, J.S., Hjelstuen, B.O., Smelror, M., Larsen, E., Andreassen, K.,
546 Eidvin, T., Vorren, T.O., 2009. The Plio-Pleistocene glaciation of the Barents Sea–Svalbard region: a new model
547 based on revised chronostratigraphy. *Quaternary Science Reviews* 28, 812-829.

548 Lund, B., Schmidt, P., 2011. Stress evolution and fault stability at Olkiluoto during the Weichselian glaciation.
549 Posiva Oy.

550 Lund, B., Schmidt, P., Hieronymus, C., 2009. Stress evolution and fault stability during the Weichselian glacial
551 cycle. Swedish Nuclear Fuel and Waste Management Co, Stockholm, Sweden.

552 Lund, B., Townend, J., 2007. Calculating horizontal stress orientations with full or partial knowledge of the
553 tectonic stress tensor. *Geophysical Journal International* 170, 1328-1335.

554 Mattingsdal, R., Knies, J., Andreassen, K., Fabian, K., Husum, K., Grøsfjeld, K., De Schepper, S., 2014. A new 6
555 Myr stratigraphic framework for the Atlantic–Arctic Gateway. *Quaternary Science Reviews* 92, 170-178.

556 Morgan, W.J., 1981. 13. Hotspot tracks and the opening of the Atlantic and Indian Oceans. *The oceanic*
557 *lithosphere* 7, 443.

558 Myhre, A.M., Eldholm, O., 1988. The western Svalbard margin (74–80 N). *Marine and Petroleum Geology* 5,
559 134-156.

560 Naliboff, J., Lithgow-Bertelloni, C., Ruff, L., de Koker, N., 2012. The effects of lithospheric thickness and
561 density structure on Earth's stress field. *Geophysical Journal International* 188, 1-17.

562 Nasuti, A., Olesen, O., 2014. Chapter 4: Magnetic data. In: Hopper J.R., Funck T., Stoker T., Arting U., Peron-
563 Pinvidic G., Doornebal H. & Gaina C. (eds) Tectonostratigraphic Atlas of the North-East Atlantic Region.
564 Geological Survey of Denmark and Greenland (GEUS), Copenhagen, Denmark, 41–51. .
565 Okada, Y., 1985. Surface deformation due to shear and tensile faults in a half-space. Bulletin of the seismological
566 society of America 75, 1135-1154.
567 Patton, H., Hubbard, A., Andreassen, K., Winsborrow, M., Stroeven, A.P., 2016. The build-up, configuration,
568 and dynamical sensitivity of the Eurasian ice-sheet complex to Late Weichselian climatic and oceanic forcing.
569 Quaternary Science Reviews 153, 97-121.
570 Petersen, C.J., Bünz, S., Hustoft, S., Mienert, J., Klaeschen, D., 2010. High-resolution P-Cable 3D seismic
571 imaging of gas chimney structures in gas hydrated sediments of an Arctic sediment drift. Marine and Petroleum
572 Geology doi: 10.1016/j.marpetgeo.2010.06.006, 1-14.
573 Planke, S., Eriksen, F.N., Berndt, C., Mienert, J., Masson, D., 2009. P-Cable high-resolution seismic.
574 Oceanography 22, 85.
575 Plaza-Faverola, A., Bünz, S., Mienert, J., 2011. Repeated fluid expulsion through sub-seabed chimneys offshore
576 Norway in response to glacial cycles. Earth and Planetary Science Letters 305, 297-308.
577 Plaza-Faverola, A., Bünz, S., Johnson, J.E., Chand, S., Knies, J., Mienert, J., Franek, P., 2015. Role of tectonic
578 stress in seepage evolution along the gas hydrate-charged Vestnesa Ridge, Fram Strait. Geophysical Research
579 Letters 42, 733-742.
580 Plaza-Faverola, A., Henrys, S., Pecher, I., Wallace, L., Klaeschen, D., 2016. Splay fault branching from the
581 Hikurangi subduction shear zone: Implications for slow slip and fluid flow. Geochemistry, Geophysics,
582 Geosystems 17, 5009-5023.
583 Plaza-Faverola, A., Vadakkepuliambatta, S., Hong, W.L., Mienert, J., Bünz, S., Chand, S., Greinert, J., 2017.
584 Bottom-simulating reflector dynamics at Arctic thermogenic gas provinces: an example from Vestnesa Ridge,
585 offshore west-Svalbard. Journal of Geophysical Research: Solid Earth.
586 Portnov, A., Vadakkepuliambatta, S., Mienert, J., Hubbard, A., 2016. Ice-sheet-driven methane storage and
587 release in the Arctic. Nature communications 7.
588 Riboulot, V., Thomas, Y., Berné, S., Jouet, G., Cattaneo, A., 2014. Control of Quaternary sea-level changes on
589 gas seeps. Geophysical Research Letters 41, 4970-4977.
590 Roy, S., Senger, K., Braathen, A., Noormets, R., Hovland, M., Olausson, S., 2014. Fluid migration pathways to
591 seafloor seepage in inner Isfjorden and Adventfjorden, Svalbard. Geological controls on fluid flow and seepage
592 in western Svalbard fjords, Norway. An integrated marine acoustic study.
593 Schiffer, C., Tegner, C., Schaeffer, A.J., Pease, V., Nielsen, S.B., 2018. High Arctic geopotential stress field and
594 implications for geodynamic evolution. Geological Society, London, Special Publications 460, 441-465.
595 Schneider, A., Panieri, G., Lepland, A., Consolaro, C., Crémière, A., Forwick, M., Johnson, J.E., Plaza-Faverola,
596 A., Sauer, S., Knies, J., 2018. Methane seepage at Vestnesa Ridge (NW Svalbard) since the Last Glacial
597 Maximum. Quaternary Science Reviews 193, 98-117.
598 Sibson, R.H., 1994. Crustal stress, faulting and fluid flow. Geological Society, London, Special Publications 78,
599 69-84.
600 Skarke, A., Ruppel, C., Kodis, M., Brothers, D., Lobecker, E., 2014. Widespread methane leakage from the sea
601 floor on the northern US Atlantic margin. Nature Geoscience 7, 657-661.
602 Smith, A.J., Mienert, J., Bünz, S., Greinert, J., 2014. Thermogenic methane injection via bubble transport into the
603 upper Arctic Ocean from the hydrate-charged Vestnesa Ridge, Svalbard. Geochemistry, Geophysics,
604 Geosystems.
605 Steffen, H., Kaufmann, G., Wu, P., 2006. Three-dimensional finite-element modeling of the glacial isostatic
606 adjustment in Fennoscandia. Earth and Planetary Science Letters 250, 358-375.

607 Svensen, H., Planke, S., Malthe-Sørenssen, A., Jamtveit, B., Myklebust, R., Eidem, T.R., Rey, S.S., 2004.
608 Release of methane from a volcanic basin as a mechanism for initial Eocene global warming. *Nature* 429, 542-
609 545.

610 Turcotte, D.L., Schubert, G., 2002. *Geodynamics*. Cambridge University Press.

611 Vanneste, M., Guidard, S., Mienert, J., 2005. Arctic gas hydrate provinces along the western Svalbard continental
612 margin. *Norwegian Petroleum Society Special Publications* 12, 271-284.

613 Vogt, P.R., Crane, K., Sundvor, E., Max, M.D., Pfirman, S.L., 1994. Methane-generated (?) pockmarks on
614 young, thickly sedimented oceanic crust in the Arctic: Vestnesa ridge, Fram strait. *Geology* 22, 255-258.

615 Wallmann, K., Riedel, M., Hong, W., Patton, H., Hubbard, A., Pape, T., Hsu, C., Schmidt, C., Johnson, J.,
616 Torres, M., 2018. Gas hydrate dissociation off Svalbard induced by isostatic rebound rather than global warming.
617 *Nature communications* 9, 83.

618 Westbrook, G.K., Thatcher, K.E., Rohling, E.J., Piotrowski, A.M., Palike, H., Osborne, A.H., Nisbet, E.G.,
619 Minshull, T.A., Lanoiselle, M., James, R.H., Huhnerbach, V., Green, D., Fisher, R.E., Crocker, A.J., Chabert, A.,
620 Bolton, C., Beszczynska-Moller, A., Berndt, C., Aquilina, A., 2009. Escape of methane gas from the seabed
621 along the West Spitsbergen continental margin. *Geophysical Research Letters* 36, 5.

622 Zoback, M.D., Zoback, M.L., 2002. 34 State of stress in the Earth's lithosphere. *International Geophysics* 81,
623 559-XII.

624